

## Preferential transport of swimmers in heterogeneous two-dimensional turbulent flow

Xinyu Si  and Lei Fang <sup>\*</sup>*Department of Civil and Environmental Engineering, University of Pittsburgh,  
Pittsburgh, Pennsylvania 15261, USA* (Received 25 April 2022; accepted 8 September 2022; published 27 September 2022)

We investigate the performance of active swimmers in a strongly heterogeneous two-dimensional weakly turbulent flow. The flow is heterogeneous in Reynolds number along one direction. Using a hybrid experimental-numerical model, we demonstrate that there are three regimes of preferential transport for rodlike swimmers as the swimmers' intrinsic speed increases. Using Lagrangian statistics along swimmers' trajectories, we reveal that the three regimes are due to the relative strengths of three different effects: the intrinsic speed of the swimmers, the reorientation ability of the shear layer at the interface of two flow regions, and the attracting Lagrangian coherent structures of the flow field. Our results elucidate the mechanism of preferential transport for swimmers in heterogeneous flow. We hope to raise researchers' attention to the dynamics of swimmers in strongly heterogeneous flow environments.

DOI: [10.1103/PhysRevFluids.7.094501](https://doi.org/10.1103/PhysRevFluids.7.094501)

### I. INTRODUCTION

The transport of swimming particles in a complex background flow is important for areas ranging from aquatic ecology [1–3] and active matter system [4–6] to bioinspired design [7,8]. Apart from considerable intrinsic mobility, these organisms are also universally featured with nonspherical shapes. Unlike passive spherical tracers, active nonspherical swimmers do not follow the flow exactly due to their shapes and intrinsic mobility.

Previous works on swimming particles in a complex background flow have found that the diffusion of swimming particles can be lower than passive particles because swimmers with small intrinsic mobility can enter and be trapped by elliptical islands [9]. At higher intrinsic mobility, researchers have found that there exists a threshold swimming velocity above which there are no barriers to the transport of swimmers. Moreover, this threshold is a function of the swimmer's shape [10]. In addition, hydrodynamic shear [11] and flow velocity [12] can have nontrivial effects on the orientation and spatial distribution of swimmers due to their intrinsic mobility and shapes, where rodlike swimmers preferentially align with flow velocity [12] and the fluid shear can trap swimmers [11]. For gyrotactic swimmers that have a preferred swimming direction, it is found that the coupling of swimmer mobility and shear can cause clustering in thin horizontal layers [13] and microscale patchiness [14]. Finally, it is shown that the attracting Lagrangian coherent structures (LCSs) have a particularly prominent effect on the preferential alignment and heterogeneous distribution for nonspherical swimmers. The mechanism of the preferential alignment between swimmers and attracting LCSs are revealed in a numerical study of swimmers in a two-dimensional turbulent flow [15].

---

<sup>\*</sup>lei.fang@pitt.edu

In general, clustering and patchiness are much weaker in three-dimensional isotropic turbulence than that observed in simple cellular or vortical flows [9,10] due to the complex topology [16]. Despite a weaker effect, turbulence can also cause swimmers to distribute heterogeneously [14,17,18]. Swimmers tend to sample regions with lower fluid vorticity and accumulate at the low vorticity regions [18]. In addition, spherical swimmers show a stronger clustering effect than elongated swimmers in isotropic turbulence [16]. It is also found that elongation as a consequence of chain formation can enhance the vertical migration of motile phytoplankton through weak to moderate turbulence [19].

Previous works have predominantly focused on the dynamics of swimmers that are surrounded by homogeneous flows or periodic flows, such as isotropic two-dimensional and three-dimensional flows and cellular flow. However, in reality, most of the swimmers are living in systems with strong heterogeneity [11,20,21].

Here, we study the preferential transport of swimmers in a flow that is strongly heterogeneous in Reynolds numbers along one direction using a hybrid experimental-numerical model [15]. In this paper, we report three regimes of the preferential transport for rodlike swimmers between two regions of two-dimensional turbulent flows with different flow intensities. While the two regions have different Reynolds numbers, the flow field is smooth everywhere. The swimmers can move with different intrinsic speeds and can be passively rotated by the flow field. At small to intermediate intrinsic speed, rodlike swimmers show a preferential transport to the faster side of the flow. We claim that it is due to the combined effects of attracting LCSs and the shear layer at the interface of the two flows. As the intrinsic speed increases, the swimmers shift the preferred transport to the slower side. We find that this is because the shear layer loses the ability to reorient swimmers, while the attracting LCSs still have a decent effect of accumulating swimmers. As a consequence, attracting LCSs alone facilitates the transport of swimmers to the slower side. Lastly, as the intrinsic speed increases to an even larger value, both the shear layer and the LCSs lose the ability to affect the swimmers and there is no preferential transport.

We begin below by first describing the method of measuring the flow field and the hybrid experimental-numerical model in Sec. II. In Sec. III, we discuss the properties of the heterogeneous flow field and elucidate the mechanism of the preferential transport of swimmers. Lastly, in Sec. IV, we summarize our results and draw conclusions.

## II. METHOD

### A. Flow realization and measurement

We generate the quasi-two-dimensional flow in an electromagnetically forced conducting thin layer system. A schematic diagram of the apparatus is shown in Fig. 1. Similar systems have been used in many other works [15,22–25]. The outer frame of the setup is made of acrylic with lateral dimensions of  $38 \times 33$  in.<sup>2</sup> ( $96.5 \times 83.8$  cm<sup>2</sup>); it supports a smooth and flat glass floor at the center with the dimension of  $32 \times 32$  in.<sup>2</sup> ( $81.3 \times 81.3$  cm<sup>2</sup>). The upper side of the glass floor is coated with hydrophobic materials (Rain-X) to reduce friction and the bottom side is covered with light-absorbing black-out film. Beneath the glass floor lies an acrylic board that can hold an array of  $29 \times 29$  cylindrical magnets with the center to center space of 1 in. (2.54 cm). Each magnet (neodymium grade N52) with an outer diameter of 0.5 in. (1.27 cm) and thickness of 0.25 in. (0.635 cm) has a maximum magnetic flux density of 1.5 T at the magnetic surface. We load a thin layer of 14% by mass NaCl solution with density  $\rho = 1.101$  g/cm<sup>3</sup> and viscosity  $\nu = 1.25 \times 10^{-2}$  cm<sup>2</sup>/s. A pair of copper electrodes are placed at opposite sides of the setup. By passing a dc current through the conducting layer, we are able to drive a quasi-two-dimensional flow with the Lorentz body force in horizontal directions. The Lorentz force is large enough to generate weakly turbulent flow, while small enough to keep the two-dimensionality.

In order to create a strongly heterogeneous flow, we put a piece of 0.25 in. (0.635 cm) thick acrylic board to fully cover the left half of the glass floor to increase bottom friction [25]. Meanwhile, the right half of the setup is fully placed with magnets, while the left half is only placed

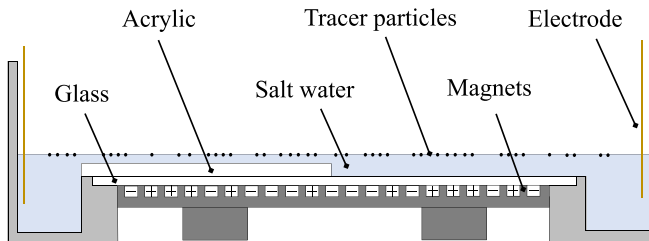


FIG. 1. Schematic for the experimental setup. The pair of electrodes conduct dc current horizontally through the saltwater. The vertical magnetic field from the permanent magnets and the horizontal dc current together generate the Lorentz force on the fluid that is nearly entirely in the plane. The fluid layer has a very high aspect ratio that can be considered as quasi-two-dimensional. A piece of acrylic board is put above the left half of the setup to increase bottom friction. The quantity of magnets in the left half is only 1/5 of that in the right half, so that the energy injection in the left half is reduced. The reduced energy injection as well as the increased friction damping make root mean square velocity of the left hand side flow much smaller than that of the right hand side flow.

with 1/5 the number of magnets in the right half. Magnets in both halves are randomly arranged and have equal numbers of opposite poles facing upward. The thicknesses of the conducting layer in the two halves are measured to be 9 mm and 2 mm, respectively. In this way, both the strength of dissipation and energy injection are different on two sides of the flow and the resulting flow is highly heterogeneous.

To track the fluid motion, the working fluid is seeded with green fluorescent polyethylene particles (Cospheric) with a density of  $1.025 \text{ g/cm}^3$  and diameters ranging from 106 to  $125 \mu\text{m}$ . The Stokes number is of order  $10^{-3}$ , which means the particle can accurately track the flow [26,27]. The tracers stay at the surface of the thin layer, which is the two-dimensional plane we study. A small amount of surfactant is added to reduce the surface tension and the surface tension is too small to affect the movement of the tracers. We use a machine vision camera (Basler, acA2040-90 $\mu\text{m}$ ) to image the particles illuminated with green LED lights. A  $1600 \text{ pixels} \times 1600 \text{ pixels}$  frame size gives a  $23 \text{ cm} \times 23 \text{ cm}$  area at the center (70 pixels/cm). About 11 000 particles can be recorded with a frame rate of 60 frames per s. The particle number density and frame rate enables us to obtain a highly spatiotemporally resolved Eulerian velocity field through a particle tracking velocimetry (PTV) algorithm, which has been described in detail elsewhere [28]. The mean distance between neighbor particles is  $d = 0.22 \text{ cm}$ , which is one order of magnitude smaller than the smallest energy injection length scale (2.54 cm). And the frame rate is two orders of magnitude smaller than the eddy turnover time. In two-dimensional flow, most of the flow dynamics take place in scales greater than the energy injection length scale due to the inverse energy cascade, where the spectral energy is fluxed toward larger scales rather than smaller scales [29].

To ensure a reliable two-dimensionality, we further project the measured flow field onto a basis of numerically computed stream function Fourier modes [22]. The projection reveals that the energy associated with out-of-plane motion is negligible, indicating our assumption of two-dimensionality is valid. The measured flow is then interpolated onto regular Eulerian grids using cubic interpolation with grid size  $\Delta x = 10 \text{ pixels}$  (0.14 cm), which is of a similar order of magnitude as  $d$ .

In this work, the root mean square velocity of the flow field is measured to be  $1.5 \text{ cm/s}$  ( $U_f$ ) in the right (faster) half and  $0.6 \text{ cm/s}$  ( $U_s$ ) in the left (slower) half. The integral length scales for the right half ( $\mathcal{L}_f$ ) and left half ( $\mathcal{L}_s$ ) are 2.5 cm and 1.0 cm, respectively. As a result, the Reynolds number  $\text{Re} = U_f \mathcal{L}_f / \nu$  for the faster side is 300 and the Reynolds number for the slower side is 48.

## B. Hybrid experimental-numerical model

We seed virtual swimmers to the measured flow field. Swimmers are modeled as inertialess, noninteracting, and pointlike ellipsoids that swim in their major axis directions  $\mathbf{p}$  with intrinsic

velocity magnitude  $v_s$ . Simultaneously, the swimmers are advected by the local flow velocity  $\mathbf{u}$  and oriented by local flow vorticity  $\boldsymbol{\omega}$  and local rate of strain tensor  $\mathbf{E}$  following Jeffery's equation [30,31]. Local  $\mathbf{u}$ ,  $\boldsymbol{\omega}$ , and  $\mathbf{E}$  are obtained through cubic interpolation of the measured flow data in Sec. II A. Consequently, we have the motion of swimmers as

$$\begin{aligned}\dot{\mathbf{x}} &= \mathbf{u}(\mathbf{x}, t) + v_s \mathbf{p}, \\ \dot{\mathbf{p}} &= \frac{1}{2} \boldsymbol{\omega} \times \mathbf{p} + \alpha \mathbf{p} \cdot \mathbf{E} \cdot (\mathbf{I} - \mathbf{p}\mathbf{p}),\end{aligned}\tag{1}$$

where the overdot represents the Lagrangian derivative,  $\mathbf{x}$  is the location of swimmers,  $\mathbf{I}$  is the identity matrix,  $\mathbf{E} = (\nabla \mathbf{u} + \nabla \mathbf{u}^T)/2$  is the strain-rate tensor,  $\boldsymbol{\omega} = \nabla \times \mathbf{u}$  is the flow vorticity, and  $\alpha = (\gamma^2 - 1)/(\gamma^2 + 1)$  is the eccentricity with  $\gamma$  the ratio between the major and minor axis of the swimmers. When  $\alpha = 0$ , the particle is spherical and when  $\alpha = 1$  the particle is an infinitely thin line segment. Jeffery's equation essentially states that, together with responding to local vorticity, swimmers with higher eccentricity also have stronger responses to the flow's local rate of strain.

The trajectories of swimmers are integrated with a second-order Runge-Kutta scheme in MATLAB. The time step,  $\Delta t = 1/60$  s, is the same as the time gap between two frames of the experimental measurement. The time step is small enough to prevent overshoot problems when solving Jeffery's equation because the Courant number  $C = U_f \Delta t / \Delta x = 0.18$  is much smaller than 1. We initiate 15 000 swimmers uniformly in the domain with random initial directions. At the end of each time step, for swimmers that leave the domain through the right half of the outer boundary, we randomly assign them back to the edge of the right half domain with random directions. Swimmers leaving the domain through the left half of the outer boundary are treated the same way. Our boundary condition limits the exchange of the virtual swimmers between the two flow regions to happen only through the interface. The system can be seen as two infinitely large flow regions which are connected via a finite length interface. Since our boundary condition reinforces the number of the swimmers in the domain to be a constant and the exchange between the two flow regions can only happen via the finite interface, the preferential transport direction of swimmers will be reflected by the concentration difference between the two flow regions when the system reaches a statistically stationary state. Therefore, we use the time-averaged swimmer concentration ratio between the faster side and the slower side under a statistically stationary state as a proxy to indicate the probability of swimmers going from the slower side to the faster side. We run the simulation for 8000 time steps (80 eddy turnover time of the faster side; the system reaches a statistically stationary state after about 3000 time steps) and the Lagrangian trajectory history for each individual swimmer is recorded.

### C. Finite time Lyapunov exponent (FTLE)

FTLE method is one of the most commonly used methods for the detection of LCSs [32]. We compute the FTLE in 2D space for the flow field following the method by Haller [32]. The flow map gradient  $\nabla F_{t_0}^t(\mathbf{x}_0)$  is calculated using finite difference approximation as

$$\nabla F_{t_0}^t(\mathbf{x}_0) \approx \begin{pmatrix} \frac{x(t; t_0, \mathbf{x}_0 + \delta_1) - x(t; t_0, \mathbf{x}_0 - \delta_1)}{2\delta_1} & \frac{x(t; t_0, \mathbf{x}_0 + \delta_2) - x(t; t_0, \mathbf{x}_0 - \delta_2)}{2\delta_2} \\ \frac{y(t; t_0, \mathbf{x}_0 + \delta_1) - y(t; t_0, \mathbf{x}_0 - \delta_1)}{2\delta_1} & \frac{y(t; t_0, \mathbf{x}_0 + \delta_2) - y(t; t_0, \mathbf{x}_0 - \delta_2)}{2\delta_2} \end{pmatrix},$$

where  $F_{t_0}^t(\mathbf{x}_0) = \mathbf{x}(t; t_0, \mathbf{x}_0)$  represents the flow map that depicts the advection of fluid particles from their initial locations  $\mathbf{x}_0$  at time  $t_0$  to their new positions  $\mathbf{x}$  at time  $t$ .  $\delta_1$  and  $\delta_2$  represent small perturbations on initial locations in  $x$  and  $y$  directions. The right Cauchy-Green tensor

$$C(\mathbf{x}_0) = [\nabla F_{t_0}^t(\mathbf{x}_0)]^T \nabla F_{t_0}^t(\mathbf{x}_0)$$

depicts how an infinitesimal perturbation evolves with time. Since  $C$  is symmetric and positive definite, the eigenvalues of  $C$ ,  $\lambda_1$ , and  $\lambda_2$  satisfy  $0 < \lambda_1 < 1 < \lambda_2$ . Then, the FTLE is calculated as

$$\text{FTLE}(\mathbf{x}_0) = \frac{1}{t - t_0} \ln \sqrt{\lambda_2(\mathbf{x}_0)}.$$

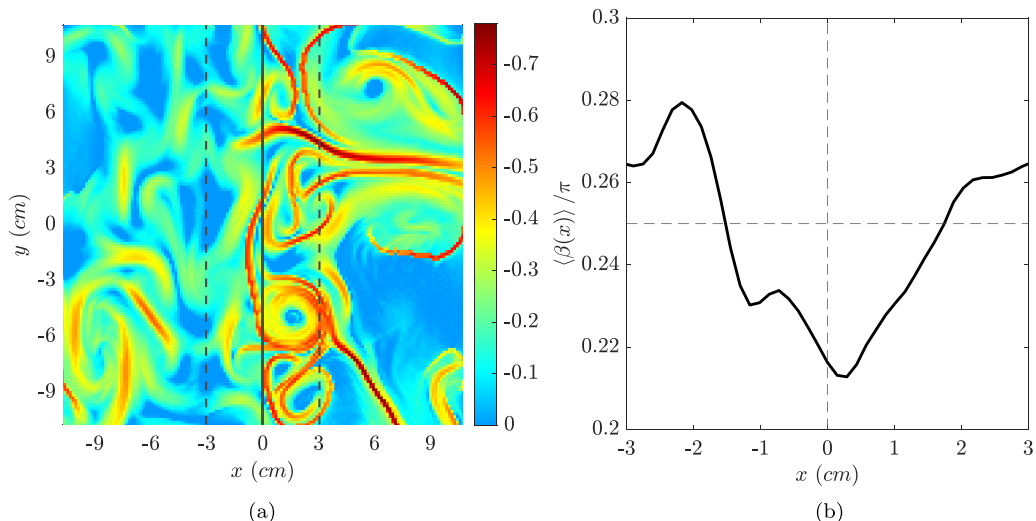


FIG. 2. (a) Snapshot of  $\text{FTLT}^-$  field, where the color bar shows local  $\text{FTLT}^-$  values (negative). Larger absolute  $\text{FTLT}$  values indicate stronger dynamics. The solid line is the middle interface. Dash lines roughly mark the boundaries of the shear layer.  $\text{FTLE}$  has a unit of  $s^{-1}$ . (b) The angle  $\beta$  between the middle interface ( $y$  axis) and the eigenvectors corresponding to the larger eigenvalues of local strain rate tensors, averaged over time and  $y$  direction.

The flow map can be traced in either forward time or backward time. The  $\text{FTLE}$  calculated with forward time integration is positive and is denoted as  $\text{FTLE}^+$ ; the  $\text{FTLE}$  calculated with backward integration is negative and is denoted as  $\text{FTLE}^-$ . Regions with extreme values are usually organized as ridges in two dimension [32,33].  $\text{FTLE}^+$  ridges and  $\text{FTLE}^-$  ridges are typically considered as effective detection for repelling and attracting LCSs.

In this paper, we take the magnitudes of both  $\delta_1$  and  $\delta_2$  to be 10 pixels (0.14 cm). The integration time length is 5 s (three eddy turnover time of the faster side). The calculation of  $\text{FTLE}$  is robust and is not sensitive to small changes of the integration time length.

### III. RESULT AND DISCUSSION

#### A. Asymmetric LCS distribution and a shear layer at interface

Due to the strong heterogeneity of the flow velocity, we observe the asymmetric distribution of attracting LCSs. Previous works have revealed that attracting LCSs have a much stronger effect on reorientating and accumulating swimmers than repelling LCSs [15,34–37], so we focus on attracting LCSs for the rest of the paper. Figure 2(a) shows a single snapshot of  $\text{FTLE}^-$  field, where the ridges are the approximated locations of LCSs [15,38]. For a given integration time, the right half region with higher flow velocity has more well-defined LCSs than the left half. It is worthwhile to note that the strong LCSs in the faster half do not end right at the middle interface but extend to the slower half to a limited length. This is because the fluid field is continuous and the flow momentum is diffused and advected from the faster side to the slower side.

Meanwhile, near the middle interface, the strong velocity difference between two sides invokes the formation of shear flows tangent to the interface. Figure 2(b) shows the temporally averaged angle  $\beta$  between the  $y$  direction and the eigenvectors corresponding to the larger eigenvalues of the local rate of strain tensors (extensional eigenvectors).  $\beta$  ranges from 0 to  $\pi/2$  and an average smaller than  $\pi/4$  suggests that extensional eigenvectors of the local rate of strain tensors tend to align with the  $y$  direction. It can be noticed that, within a 2 to 3 cm band near the interface, the averaged

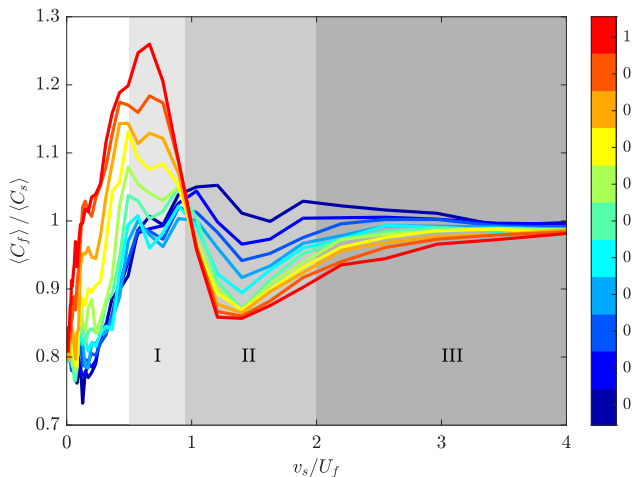


FIG. 3. Ratio between the time-averaged swimmer density in the faster side ( $\langle C_f \rangle$ ) and the time-averaged swimmer density in the slower side ( $\langle C_s \rangle$ ). From blue to red, the  $\alpha$  of swimmers increases from 0 to 1.

$\beta$  decreases as it approaches the interface from both sides, which indicates the existence of the shear layer.

From Jeffery's equation [30,31], we know that rodlike swimmers ( $\alpha > 0$ ) tend to rotate to align with extensional eigenvectors of the local rate of strain tensors. Moreover, it is found that the alignment between rodlike swimmers and LCSs is more prominent than that between swimmers and the extensional rate of strain eigenvectors [15,39]. In the following two sections, we will demonstrate that the intrinsic speed of swimmers, the reorientation ability of the shear layer at the interface of two flow regions, and the attracting LCSs conspire to lead to three distinct regimes of the preferential transport of swimmers in the heterogeneous two-dimensional turbulent flow based on the relative strengths of the three effects.

### B. Three regimes of the preferential transport of nonspherical swimmers

We calculate the ratio between the time-averaged swimmer density in the faster side ( $\langle C_f \rangle$ ) and that in the slower side ( $\langle C_s \rangle$ ) for swimmers with different  $v_s$  and  $\alpha$  after the simulation reaches a statistically stationary state (Fig. 3). For elongated swimmers, as  $\alpha$  increases, the  $\langle C_f \rangle / \langle C_s \rangle$  ratio shows three distinct regimes of preferential transport (Fig. 3). We claim that these three regimes result from the relative strengths of three different effects: the intrinsic speed of the swimmers (effect 1), the reorientation ability of the shear layer (effect 2) at the interface of two flow regions, and the attracting LCSs (effect 3). In the range of  $v_s$  between  $0.5U_f$  and  $1U_f$ , the swimmers have preferential transport toward the faster side (regime I; effect strength in increasing order: effect 1, effect 2, effect 3). As  $v_s$  increases to the range between  $1U_f$  and  $2U_f$ , they have preferred transport to the slower side (regime II; effect strength in increasing order: effect 2, effect 1, effect 3). When  $v_s$  is greater than  $2U_f$ , the preferential transport gradually disappears, and there will be no preferential transport in the heterogeneous flow (regime III; effect strength in increasing order: effect 2, effect 3, effect 1).

One thing to note is that, for the tracer case ( $v_s = 0$ ), the simulation shows a preferential transport toward the slower region. In our experiment, we measured only a subsection of the interface. At a steady state, the transport of tracers toward each side should be the same along the whole interface, but it is not necessarily true for a subset of the interface. Hence we determine that this is due to the limited size of the measurement domain, limited Reynolds numbers, combined with the numerical boundary conditions we use and the arrangement of finite-numbered magnets. As the intrinsic speed

of the swimmers increases, the interaction between the intrinsic mobility of swimmers and the flow becomes dominant and the effect that results from the boundary conditions becomes negligible. This can be validated by looking at the behavior of concentration ratio for spherical swimmers with increasing intrinsic speed ( $\alpha = 0$ , dark blue curve). As  $v_s$  increases, the concentration ratio quickly converges to 1, as it should.

In the following of this paper, we will use rodlike swimmers ( $\alpha = 1$ ) as an example for discussions because they show the strongest effect.

In regime I ( $v_s$  between  $0.5U_f$  and  $1U_f$ ), due to the intermediate intrinsic velocity of the swimmers, both LCSs and the shear layer have significant effects on the swimmers' movement. Even with an intermediate intrinsic velocity, swimmers in the slower side of the flow become less dependent on the flow and will approach a uniform distribution. However, in the faster side, within the range of swimming velocity between  $0.5U_f$  and  $1U_f$ , swimmers show a strong preferential alignment and heterogeneous distribution near LCSs [15]. A great portion of swimmers in the faster flow region are swimming along LCSs. Since LCSs extend through the middle interface into the slower region [Fig. 2(a)], swimmers will swim along these LCSs both toward and away from the interface. Additionally, there exists a shear layer tangent to the middle interface. For the swimmers swimming toward the slower side along the LCSs, the shear layer reorientates the swimmers to the direction tangent to the middle interface, which increases the probability for those swimmers to encounter another LCS where the local flow field points back to the faster side. Hence swimmers in the faster side of the flow will have a higher chance to go back to the faster side once they reach the vicinity of the interface. We call this phenomenon "swimmer recycling." The recycling requires both the shear layer at the interface and LCSs with local flow velocities pointing back toward the faster side (see schematic in Fig. 4). Since there is no definite LCS in the slower side for the time scale we consider, there will be no recycling mechanism and, consequently, the LCSs with local flow velocities pointing toward the faster side will keep guiding the swimmer from the slower side to the faster side. Thus, when  $v_s$  is between  $0.5U_f$  and  $1U_f$ , the rodlike swimmer is preferentially transported toward the faster side of the flow.

In regime II ( $v_s$  between  $1U_f$  and  $2U_f$ ), the intrinsic speed of swimmers is strong enough to overcome the weaker realignment effect of the shear layer at the interface. Even though the alignment and accumulation effects of the LCSs start to weaken, there are still a substantial amount of swimmers that swim along the LCSs. Since the reorientation of the shear layer is the key step in the recycling mechanism and it is significantly weakened in regime II, swimmer recycling is weak in this regime. Without the swimmer recycling, the LCSs in the faster side then serve to facilitate the transport of swimmers from the faster side to the slower side, resulting in the preferential transport toward the slower side of the flow.

In regime III ( $v_s$  greater than  $2U_f$ ), the swimmers' intrinsic speed continues to increase and both LCSs and the shear layer have negligible effects on the swimmers. Therefore, the concentration ratio gradually approaches 1.

One thing to note is that, for very slow spherical swimmers (around  $v_s/U_f = 0.2$  and  $\alpha = 0$ ), the concentration ratio shows a weak descending trend compared with that for tracers. This might result from the trapping effect near the elliptical region in the slower side. Khurana *et al.* [9] found that swimming does not necessarily enhance swimmer transport. By advecting spherical swimmers in a 2D cellular flow, they showed that small but finite swimming speed could cause swimmers to get stuck for long times near elliptical islands. Here in our measured flow, there also exists long-lasting elliptical structures that can possibly result in similar trapping effects as that in Khurana *et al.* [9].

### C. Lagrangian statistics for preferential transport

To support our mechanistic picture, we start to investigate the Lagrangian statistics for swimmers in both sides of the flow that are within a 3 cm distance from the middle interface, where the effects of both the shear layer and the LCSs are substantial. Our result is consistent for any reasonable range of distance near the interface.

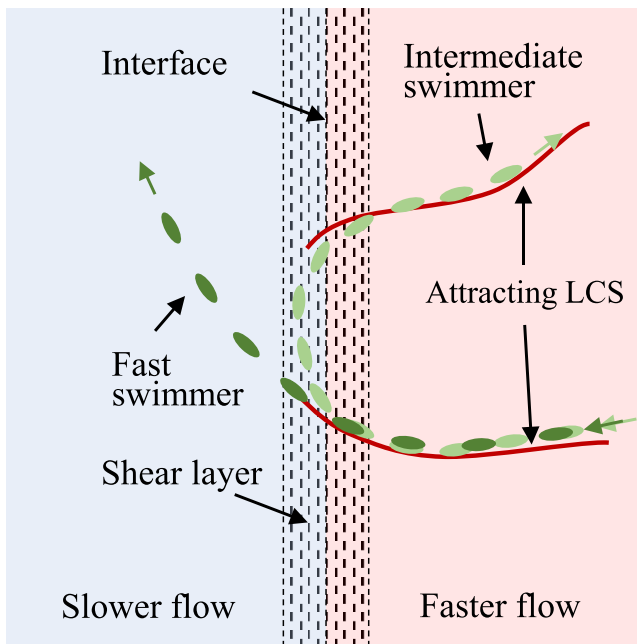


FIG. 4. Schematic for the effect of LCSs and the shear layer on rodlike swimmers at different regimes. The intermediate swimmer (light green) is at regime I and it is affected by both LCSs and the shear layer. Once it walks on an LCS to reach the interface, it is reoriented by the shear layer and encounters another nearby LCS where local velocity points toward the faster side. Thus recycling is completed. The fast swimmer (dark green) is in regime II and it is only affected by the LCSs. In this case, LCSs on the faster side facilitate the preferential transport toward the slower side. Once the swimmers' intrinsic velocity increase and reach regime III, the flow will have a negligible effect on the swimmers and preferential transport will disappear.

We first examine the response of swimmer motions toward attracting LCSs near the interface. We sample equal numbers of swimmers uniformly at both sides of the interface and look at the  $FTLE^-$  values along their trajectories. As time moves forward, we keep tracking the normalized ensemble average of local  $FTLE^-$  values for swimmers that still remain in the domain of interest [Fig. 5(a)]. Comparing the swimmers starting from the slower and faster sides, we see that, for both swimmers with  $v_s = 0.7U_f$  and  $v_s = 1.4U_f$ , the normalized ensemble average of local  $FTLE^-$  keeps increasing for swimmers starting from the faster side. But for swimmers in the slower side, the normalized ensemble average of local  $FTLE^-$  does not show significant changes with the change of time. This means that the retained swimmers are closely related to LCSs in the faster flow region but are not affected by LCSs in the slower flow region because the slower side does not have definite LCSs for the time scale we consider. This result suggests that the retained swimmers starting from the faster flow region tend to sample higher  $|FTLE^-|$  (the vicinity of attracting LCSs) and, thus, indicates that LCSs play a key role in recycling swimmers in the faster flow region. Moreover, the lower increasing trend for swimmers with  $v_s = 1.4U_f$  indicates the weakened accumulation effect of LCSs for swimmers. Note that this is not direct evidence for the swimmer recycling but a consequence of the recycling. In the following, we will show evidence for each component of the recycling mechanism.

We then reveal how the shear layer reorients swimmers clustered on the LCSs in the faster side. In doing so, we specifically condition on the swimmers that (1) are near the vicinity of LCSs and (2) have intrinsic speed pointing toward the slower side. Swimmers in the right (faster) 3 cm band with local  $|FTLE^-|$  higher than 0.4 and  $x$  component of  $\mathbf{p}$  pointing to the left (slower side) at  $t = 0$  are

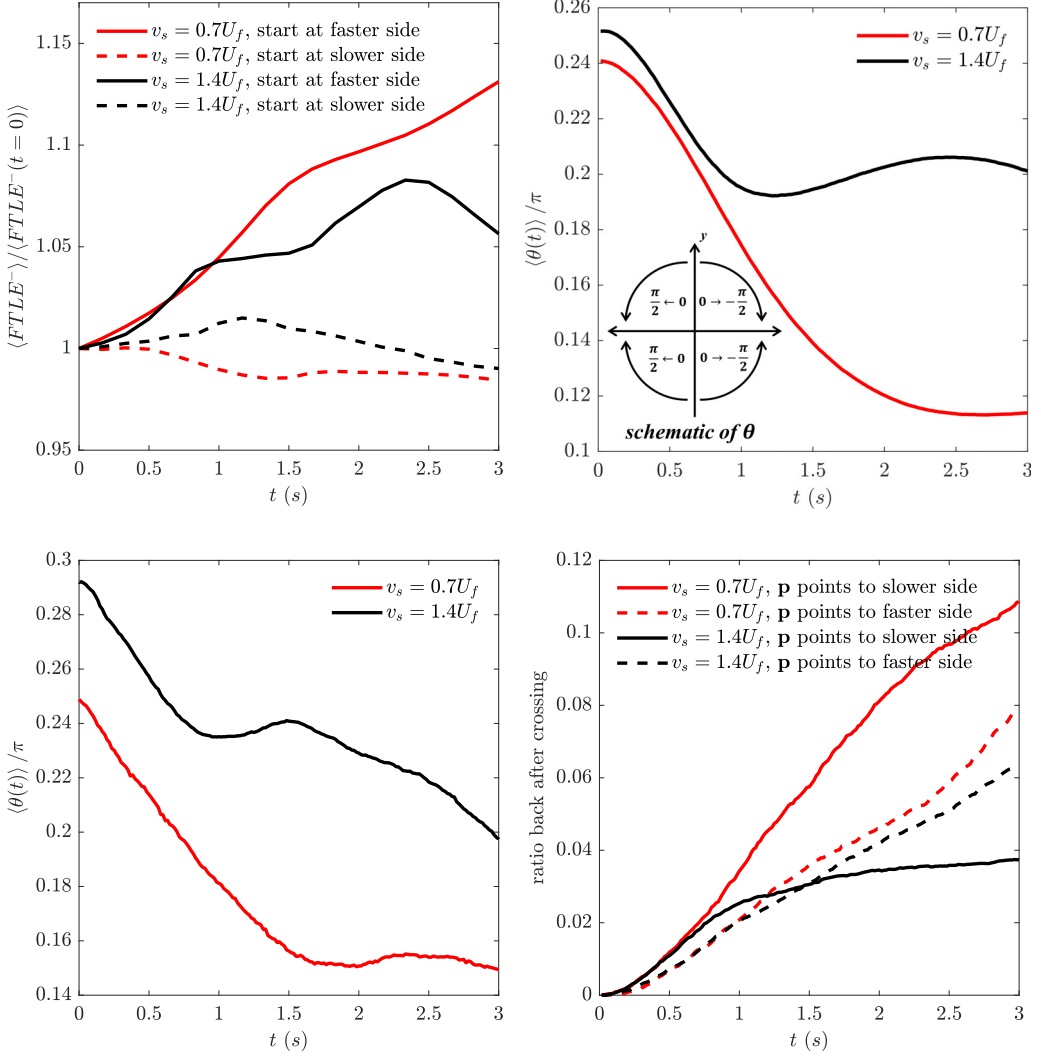


FIG. 5. (a) Time-averaged local FTLE<sup>-</sup> values for swimmers stay in the band within 3 cm distance from the middle interface, normalized by the initial averaged FTLE<sup>-</sup>. (b) The forward time Lagrangian statistics of the angle  $\theta$  between the middle interface ( $y$  axis) and the orientation of swimmers  $\mathbf{p}$  for swimmers that are in the right 3 cm band and have the  $x$  component of  $\mathbf{p}$  pointing toward the left at  $t = 0$ . If the  $x$  component of  $\mathbf{p}$  is pointing toward the right (faster side),  $\theta$  is considered as negative; if the  $x$  component of  $\mathbf{p}$  is pointing toward the left (slower side),  $\theta$  is considered as positive. The subfigure shows the schematic of calculating  $\theta$ . (c) The forward time Lagrangian statistics of  $\theta$  for swimmers that cross the interface at  $t = 0$  from the faster side to the slower side. Panels (b) and (c) show that the shear layer is effective in reorienting swimmers with  $v_s = 0.7U_f$  (in regime I) but not in reorienting swimmers with  $v_s = 1.4U_f$  (in regime II). (d) The ratio of swimmers that return to their original side when they cross the middle interface at  $t = 0$ . The direction of  $\mathbf{p}$  in the legend indicates the direction of  $v_s$  when swimmers cross the interface at  $t = 0$ .

selected out. The specific threshold of FTLE<sup>-</sup> does not affect our result. We calculate the forward time Lagrangian statistics of the angle  $\theta$  between the middle interface ( $y$  axis) and the orientation of swimmers  $\mathbf{p}$  [Fig. 5(b)]. If the  $x$  component of  $\mathbf{p}$  is pointing left,  $\theta$  is recorded to be positive; if the  $x$

component of  $\theta$  is pointing right,  $\theta$  is recorded to be negative. Therefore,  $\theta$  ranges from  $-\pi/2$  to  $\pi/2$  and  $\langle\theta\rangle$  closer to zero indicates that the swimmers are more tangential to the  $y$  axis. When swimmers approach the middle interface, for both swimmers with  $v_s = 0.7U_f$  and  $v_s = 1.4U_f$ , the mean angle decreases. A similar trend indicates that swimmers with both velocities can be reoriented by the shear layer. Despite the similar trend, swimmers with  $v_s = 0.7U_f$  show a sharper decrease and a much smaller  $\langle\theta\rangle$  than swimmers with  $v_s = 1.4U_f$ , which indicates that the shear layer has a more prominent effect on reorienting intermediate swimmers ( $v_s = 0.7U_f$ ). A great portion of swimmers swimming along LCSs toward the interface is realigned and recycled to their original domain. For swimmers with  $v_s = 1.4U_f$ , it can be noticed that, even though the shear layer tends to align the swimmers to be parallel to the  $y$  axis, the effect is very limited. A mean angle that doubles the  $\langle\theta\rangle$  for swimmers with  $v_s = 0.7U_f$  indicates that most swimmers cannot be reoriented to the tangent direction of the interface. This makes the recycling of faster swimmers ( $v_s = 1.4U_f$ ) much more difficult than that of swimmers with  $v_s = 0.7U_f$ . This result shows that the shear layer can reorient swimmers on LCSs toward the slower side for the swimmers in regime I but not for swimmers in regime II.

To further reveal the effect of the shear layer for any swimmers that cross the interface toward the slower side, in Fig. 5(c), we show the forward time Lagrangian statistics of the angle  $\theta$  for all swimmers that cross the middle interface from the faster side to the slower side at  $t = 0$ . Therefore, in this case, swimmers both near LCSs and away from LCSs are included. We can observe that Fig. 5(c) shows a similar trend as Fig. 5(b). However, since the off-LCSs swimmers are moving in a more random manner, the decreasing of  $\langle\theta\rangle$  in Fig. 5(c) is slower than Fig. 5(b). Also, a mean angle greater than  $\pi/4$  for swimmers with  $v_s = 1.4U_f$  near  $t = 0$  indicates that most swimmers are swimming in a normal direction with respect to the middle interface rather than in the tangent direction when crossing the interface. Figures 5(b) and 5(c) together reveal that the shear layer has a decent effect on reorienting swimmers to be parallel to the interface in regime I but not in regime II.

After showing the effect of LCSs and the shear layer, we now demonstrate that the recycling of the swimmers indeed exists. We calculate the ratio of the swimmers that return to their original side (“recycling”) in forward time for swimmers that pass the middle interface at  $t = 0$  [Fig. 5(d)]. In the slower side, swimmers with both  $v_s = 0.7U_f$  and  $v_s = 1.4U_f$  have similar ratios of returning their original domain (slower side) because LCSs, as one of the key components for swimmer recycling, are less prominent in the slower side during the time scale that we consider. Moreover, in both cases, the swimmers’ intrinsic velocities are faster than the root mean square velocity of the flow in the slower side; hence swimmers at both intrinsic velocities are uniformly distributed in the slower side. This confirms that the recycling mechanism is missing in the slower side. For swimmers that originate from the faster side, however, those with  $v_s = 0.7U_f$  have a much higher ratio of returning their original domain (faster side) than those with  $v_s = 1.4U_f$ . This is because the swimmers’ intrinsic speed is small enough to be affected by both the shear layer and LCSs so that the recycling mechanism takes effect. The ratio of recycling after crossing the interface is also consistent with the results in Figs. 5(a), 5(b), and 5(c). For swimmers with  $v_s = 1.4U_f$ , we see that the return ratio is the lowest. This is because the swimmers’ mobility is strong enough to overcome the realignment effect of the shear layer [Figs. 5(b) and 5(c)] but not strong enough to overcome the effect of LCSs [15]. In this case, the LCSs are facilitating the transport of swimmers from the faster side to the slower side. This result is consistent with our explanation in Sec. III B that the recycling mechanism only happens to swimmers that start from the faster side and only for those affected by both the shear layer and LCSs, i.e., in regime I. Note that recycling does not only happen at a small band on the interface; it happens over a pretty broad range around the interface.

#### IV. CONCLUSION

We examined the preferential transport of active swimmers in strongly heterogeneous flow by seeding virtual swimmers to experimentally measured two-dimensional weak turbulence. Our results provided insights into the swimmer dynamics in strongly heterogeneous flow. After a brief

description of the asymmetric property of the flow field, we demonstrated that there exist three distinct regimes of preferential transport as the rodlike swimmers' intrinsic speed increases. We revealed that the three regimes are due to the relative strengths of three different effects: the intrinsic speed of the swimmers, the reorientation ability of the shear layer at the interface of two flow regions, and the attracting LCSs.

When the swimmers' intrinsic speed is small, and the reorientation ability of both the shear layer and the LCSs are strong, a recycling mechanism exists that helps to recycle the swimmers originating from the faster region back to their original domain, leading to a preferential transport toward the faster side (regime I). As the swimmers' intrinsic speed increases, the shear layer loses the ability to reorient the swimmers, and the LCSs in the faster side alone actually facilitate the preferential transport of the swimmer toward the slower side (regime II). The preferential transport gradually disappears as the swimmers' mobility increases even higher, in which case both the shear layer and the LCSs have negligible effects on the swimmers (regime III). After forming the mechanistic picture, we used Lagrangian statistics to support this mechanistic picture. We demonstrated the following. (1) The spatial distribution of swimmers near the interface is strongly correlated with LCSs in the faster side of the flow. But swimmers show no preference for the slower side of the flow. In addition, LCSs play a more prominent role for swimmers in regime I than for those in regime II [Fig. 5(a)]. (2) The shear layer reorients the swimmers to be parallel to the interface and the shear layer has a more significant effect on swimmers in regime I [Figs. 5(b) and 5(c)]. (3) There is a significant contrast between swimmers' return statistics and the contrast is consistent with the recycling mechanism [Fig. 5(d)].

Lastly, we want to raise attention to the swimmers' dynamics in strongly heterogeneous flows since many of the swimmers in natural and industrial systems are surrounded by heterogeneous flows instead of homogeneous flows. There are many open questions to answer which are outside the scope of this paper. First, what will the swimmer dynamics change when the Reynolds number ratio changes. If the Reynolds number ratio decreases, LCSs at both slower and faster sides will be similarly prominent. Then, it is unclear which regime will disappear first as the Reynolds number ratio decreases. If the Reynolds number ratio increases while there is enough dynamical range for both flow regions, there will be a case where the swimmer's intrinsic speed is low compared to both the slower flow and faster flow. New dynamics should emerge in this range according to our previous research [15] because the swimmers in the slower side will not distribute homogeneously. Currently, this range is too narrow due to the intrinsic limitation of the experiments. Moreover, the swimmers' dynamics in three-dimensional heterogeneous flow are not known. We hypothesize that it will be intrinsically distinct from the two-dimensional dynamics because LCSs, one of the critical factors in the preferential transport in two dimensions, are not stable in three dimensions.

#### ACKNOWLEDGMENT

L.F. acknowledges the start-up package and Pitt Momentum Fund at the University of Pittsburgh and the U.S. National Science Foundation under Grant No. CMMI-2143807.

- 
- [1] H. L. Fuchs and G. P. Gerbi, Seascape-level variation in turbulence-and wave-generated hydrodynamic signals experienced by plankton, *Prog. Ocean.* **141**, 109 (2016).
  - [2] J. S. Guasto, R. Rusconi, and R. Stocker, Fluid mechanics of planktonic microorganisms, *Annu. Rev. Fluid Mech.* **44**, 373 (2012).
  - [3] D. Elmi, D. R. Webster, and D. M. Fields, Response of the copepod *acartia tonsa* to the hydrodynamic cues of small-scale, dissipative eddies in turbulence, *J. Exp. Biol.* **224**, jeb237297 (2021).
  - [4] P. T. Underhill, J. P. Hernandez-Ortiz, and M. D. Graham, Diffusion and Spatial Correlations in Suspensions of Swimming Particles, *Phys. Rev. Lett.* **100**, 248101 (2008).

- 
- [5] S. C. Takatori, W. Yan, and J. F. Brady, Swim Pressure: Stress Generation in Active Matter, *Phys. Rev. Lett.* **113**, 028103 (2014).
- [6] M. C. Marchetti, J.-F. Joanny, S. Ramaswamy, T. B. Liverpool, J. Prost, M. Rao, and R. A. Simha, Hydrodynamics of soft active matter, *Rev. Mod. Phys.* **85**, 1143 (2013).
- [7] R. Dreyfus, J. Baudry, M. L. Roper, M. Fermigier, H. A. Stone, and J. Bibette, Microscopic artificial swimmers, *Nature (London)* **437**, 862 (2005).
- [8] B. ten Hagen, F. Kümmel, R. Wittkowski, D. Takagi, H. Löwen, and C. Bechinger, Gravitaxis of asymmetric self-propelled colloidal particles, *Nat. Commun.* **5**, 1 (2014).
- [9] N. Khurana, J. Blawdziewicz, and N. T. Ouellette, Reduced Transport of Swimming Particles in Chaotic Flow due to Hydrodynamic Trapping, *Phys. Rev. Lett.* **106**, 198104 (2011).
- [10] C. Torney and Z. Neufeld, Transport and Aggregation of Self-Propelled Particles in Fluid Flows, *Phys. Rev. Lett.* **99**, 078101 (2007).
- [11] R. Rusconi, J. S. Guasto, and R. Stocker, Bacterial transport suppressed by fluid shear, *Nat. Phys.* **10**, 212 (2014).
- [12] M. Borgnino, K. Gustavsson, F. De Lillo, G. Boffetta, M. Cencini, and B. Mehlig, Alignment of Nonspherical Active Particles in Chaotic Flows, *Phys. Rev. Lett.* **123**, 138003 (2019).
- [13] W. M. Durham, J. O. Kessler, and R. Stocker, Disruption of vertical motility by shear triggers formation of thin phytoplankton layers, *Science* **323**, 1067 (2009).
- [14] W. M. Durham, E. Climent, M. Barry, F. De Lillo, G. Boffetta, M. Cencini, and R. Stocker, Turbulence drives microscale patches of motile phytoplankton, *Nat. Commun.* **4**, 1 (2013).
- [15] X. Si and L. Fang, Preferential alignment and heterogeneous distribution of active non-spherical swimmers near lagrangian coherent structures, *Phys. Fluids* **33**, 073303 (2021).
- [16] C. Zhan, G. Sardina, E. Lushi, and L. Brandt, Accumulation of motile elongated micro-organisms in turbulence, *J. Fluid Mech.* **739**, 22 (2014).
- [17] K. D. Squires and J. K. Eaton, Preferential concentration of particles by turbulence, *Phys. Fluids* **3**, 1169 (1991).
- [18] N. Pujara, M. Koehl, and E. Variano, Rotations and accumulation of ellipsoidal microswimmers in isotropic turbulence, *J. Fluid Mech.* **838**, 356 (2018).
- [19] S. Lovecchio, E. Climent, R. Stocker, and W. M. Durham, Chain formation can enhance the vertical migration of phytoplankton through turbulence, *Sci. Adv.* **5**, eaaw7879 (2019).
- [20] A. Martin, Phytoplankton patchiness: the role of lateral stirring and mixing, *Prog. Ocean.* **57**, 125 (2003).
- [21] H. Yang, R. H. Weisberg, P. P. Niiler, W. Sturges, and W. Johnson, Lagrangian circulation and forbidden zone on the west florida shelf, *Contin. Shelf Res.* **19**, 1221 (1999).
- [22] D. H. Kelley and N. T. Ouellette, Onset of three-dimensionality in electromagnetically driven thin-layer flows, *Phys. Fluids* **23**, 045103 (2011).
- [23] L. Fang and N. T. Ouellette, Advection and the Efficiency of Spectral Energy Transfer in Two-Dimensional Turbulence, *Phys. Rev. Lett.* **117**, 104501 (2016).
- [24] L. Fang and N. T. Ouellette, Influence of lateral boundaries on transport in quasi-two-dimensional flow, *Chaos* **28**, 023113 (2018).
- [25] L. Fang and N. T. Ouellette, Transport across a bathymetric interface in quasi-two-dimensional flow, *Phys. Rev. Fluids* **4**, 064501 (2019).
- [26] N. T. Ouellette, P. J. J. O'Malley, and J. P. Gollub, Transport of Finite-Sized Particles in Chaotic Flow, *Phys. Rev. Lett.* **101**, 174504 (2008).
- [27] L. Fang and N. T. Ouellette, Multiple stages of decay in two-dimensional turbulence, *Phys. Fluids* **29**, 111105 (2017).
- [28] N. T. Ouellette, H. Xu, and E. Bodenschatz, A quantitative study of three-dimensional lagrangian particle tracking algorithms, *Exp. Fluids* **40**, 301 (2006).
- [29] G. Boffetta and R. E. Ecke, Two-dimensional turbulence, *Annu. Rev. Fluid Mech.* **44**, 427 (2012).
- [30] G. B. Jeffery, The motion of ellipsoidal particles immersed in a viscous fluid, *Proc. R. Soc. London Ser. A* **102**, 161 (1922).
- [31] T. Pedley and J. O. Kessler, Hydrodynamic phenomena in suspensions of swimming microorganisms, *Annu. Rev. Fluid Mech.* **24**, 313 (1992).

- [32] G. Haller, Lagrangian coherent structures, *Annu. Rev. Fluid Mech.* **47**, 137 (2015).
- [33] G. Haller and G. Yuan, Lagrangian coherent structures and mixing in two-dimensional turbulence, *Physica D* **147**, 352 (2000).
- [34] T. MacMillan and D. H. Richter, The most robust representations of flow trajectories are lagrangian coherent structures, *J. Fluid Mech.* **927**, A26 (2021).
- [35] D. H. Kelley, M. R. Allshouse, and N. T. Ouellette, Lagrangian coherent structures separate dynamically distinct regions in fluid flows, *Phys. Rev. E* **88**, 013017 (2013).
- [36] G. A. Voth, G. Haller, and J. P. Gollub, Experimental Measurements of Stretching Fields in Fluid Mixing, *Phys. Rev. Lett.* **88**, 254501 (2002).
- [37] G. Haller, Lagrangian structures and the rate of strain in a partition of two-dimensional turbulence, *Phys. Fluids* **13**, 3365 (2001).
- [38] N. T. Ouellette, C. A. Hogg, and Y. Liao, Correlating lagrangian structures with forcing in two-dimensional flow, *Phys. Fluids* **28**, 015105 (2016).
- [39] S. Parsa, J. S. Guasto, M. Kishore, N. T. Ouellette, J. Gollub, and G. A. Voth, Rotation and alignment of rods in two-dimensional chaotic flow, *Phys. Fluids* **23**, 043302 (2011).